ANNALS OF GEOPHYSICS, 62, 6, GT675, 2019; doi: 10.4401/ag-8063

"CRUSTAL STRUCTURE OF ANDAMAN ISLANDS USING JOINT INVERSION OF RECEIVER FUNCTIONS AND SURFACE WAVE DISPERSION MEASUREMENTS"

Santosh Mishra[*,1], Srichand Prajapati[2]

(1) National Geophysical Research Institute (NGRI), Hyderabad, India
(2) Centre for Seismic Imaging, Universiti Teknologi PETRONAS, Malaysia

Article history
Received December 12, 2018; accepted May 1, 2019.
Subject classification:
Andaman Islands; Subduction zone; Crustal Structure; Joint Inversion; Receiver Function; Surface Wave Dispersion.

ABSTRACT

We investigate the crustal structure of Andaman Islands, central part of Burma-Sunda-Java subduction complex, through joint inversion of receiver functions and surface wave dispersion measurements. For this study, we used teleseismic earthquakes recorded over 13 temporary broadband seismographs operated in two different phases: pre and post 2004 Sumatra earthquake. Beneath the Andaman forearc region, the crustal thickness varies between ~24 and 28 km. The uppermost crust consists of ~4 to 7 km thick soft accretionary sediments. Average Vp/Vs ratio, between ~1.79 and 1.83, suggests accretionary hydrated oceanic crust with different level of saturation. Combining derived crustal structure with global seismicity and CMT fault plane solutions indicate a complex convergence along the arc, with transitional (continental-oceanic) type in the north to oceanic type in the south Andaman.

1. INTRODUCTION

The Andaman Islands are part of the Andaman-Nicobar Ridge (ANR) which hosts Andaman and Nicobar group of Islands. These Islands mark the eastern margin of the Indian plate and form an important transitional tectonic link between the eastern Himalayan syntaxis in the north and Sunda arc in south. These represent the central part of the ~5000 km long Burma-Sunda-Java subduction complex, displaying major tectono-stratigraphic elements striking approximately parallel to the trend of subduction trench. The tectonic framework of the region has been reviewed by various researchers [e.g., Curray, 2005; Lay et al., 2005; Kamesh Raju et al., 2012 and reference within].

Global plate tectonic reconstructions suggest the complex convergence of Indian plate along Southeast Asian margin, which has resulted in clockwise rotation of the subduction zone and increase in the obliquity [Replumaz et al., 2010]. Subduction in this region is pre-

sumed to have started in lower Cretaceous [Scotese et al., 1988], which occurs all along the Sunda arc and extends from the eastern Himalayan syntaxis to Banda arc [Curray, 2005]. The age and thickness of the subducted oceanic crust and convergence rate increase from Andaman towards Java along the arc [Lay et al., 2005]. This change is observed in the increasing dip and depth of penetration of the wadati-Benioff zone, causing change in subducting slab geometry. Oblique, but predominantly thrust motion occurs in the Andaman trench with a convergence rate of about 1.4 cm/yr [Lay et al., 2005]. The convergence varies from continental type (Indian continental plate vs Burmese plate) in the Burmese arc to oceanic type (Indian oceanic plate vs Burmese plate) in the Andaman arc [Subrahmanyam et al., 2008]. It is believed that early subduction was comparatively fast which subsequently progressed in multiple episodes as short- and long-lived subduction zones converging at different rates [Richards et al., 2007]. This convergence (at variable rate, increased obliquity, dip and rotation) has resulted in development of a plate sliver that is referred as Andaman or Burmese microplate, which is a sheared off plate parallel to the subduction zone from Myanmar to Sumatra. Prominent morphological features in the region includes several sea mounts, volcanic arc, Barren Island (BaI), Narcondam Island (NaI), Andaman Backarc Spreading Center (ABSC), Alcock and Sewell seamount complexes, Backarc basin (Figure 1).

Geologically, Andaman Islands are exposed tectonostratigraphic units of an accretionary prism in an outer arc setting and turbidities of a forearc setting. Rocks in this region belong to the upper Cretaceous to Tertiary, with Oligocene flysch covering the western part and the Paleocene to Eocene sediments of Mithakari covering the eastern part. Some Ophiolites belonging to the Mesozoic lower Cenozoic also occur in small patches in different places [Pal et al., 2003].

Seismotectonics, nature of faulting and stress distribution pattern for the Andaman arc have been studied earlier [e.g. Mukhopadhyay, 1984; Guzman-Speziale and Ni, 1996; Radhakrishna and Sanu, 2002; Dasgupta et al., 2003; Khan, 2005]. Predominant seismic activity in Andaman region is attributed to subduction of In-

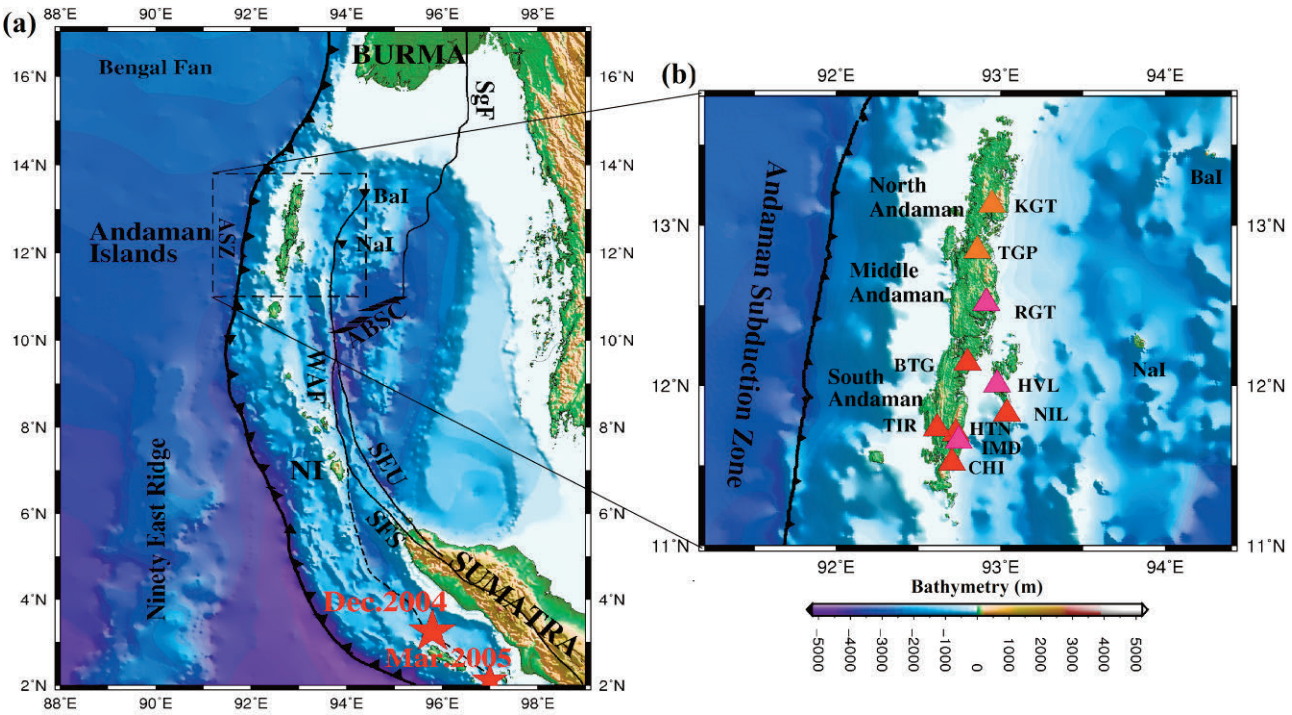

FIGURE 1. Simplified regional tectonic framework of Andaman arc–trench system, superimposed on GEBCO bathymetry and SRTM data. Major tectonic units in the region are Nicobar Island (NI), Barren Island (BaI), Narcondam Island (NaI), Andaman Backarc Spreading Center (ABSC), Andaman Subduction zone (ASZ), West Andaman Fault (WAF), Sagaing Fault (SgF), Sumatra fault system (SFS) and Seulimeum strand of SFS (SEU). Red stars show two great earthquakes on Dec–2004 (Mw 9.3) and Mar–2005 (Mw 8.6). (b) Simplified map of study region, divided into north, middle and south Andaman. The seismic stations used in this study are shown as orange (Nov 2003 – Feb 2004; phase 1) and red (Jan – May 2005; phase 2) triangles. Pink triangles are overlapped stations operated in both the phases.

dian slab which is evidenced by the several earthquakes of magnitude (M>8) on the Richter scale and intense vertical movements over the past about 200 years [Bilham et al., 2005; Engdahl et al., 2007]. The depth of the earthquakes in the region ranges between ~150 and 300 km; which seems to increase from ~150 km in Andaman region (at around 12° N) to almost ~300 km in the south (at around 4° N) [Sorensen et al., 2007)]. Tomographic images suggest subhorizontal tear in the subducting slab below Burma [Replumaz et al. 2010; Pesicek et al., 201; Mishra et al, 2020]. Curray [2005] and Mishra et al. [2011] suggest the presence of strong heterogeneity in crust and upper mantle, as the lithosphere in the Andaman sea region underwent complex tectonic deformations during the Neogene-Quaternary period.

An earthquake of Mw 9.3 (popularly known as Sumatra-Andaman Earthquake) hit the region on 26 December 2004. Several studies were carried out after this mega thrust earthquake highlighting shift in seismogenic coupling zone and ~1400 km rupture zone extending up to Andaman Islands [Kennett and Cummins, 2005; Ammon et al., 2005; Ishi et al., 2005; Grevemeyer and Tiwari, 2006; Shapiro et al., 2008]. This mega event also reactivated Barren volcanic Island which indicates the tight link between tectonics and magmatism of this complex system [Franke et al., 2008]. Ever since, this area has witnessed more than 17,000 aftershocks [Mishra et al., 2011].

Despite being one of the most active terrain and its tectonic linkage to Sumatra subduction system, so far, no systematic study related to crustal structure has been carried out particularly beneath Andaman Islands. Geographical limitation, logistic difficulties, dense forest, aboriginal reserve areas could be possible reasons. To study the crust - upper mantle structure and seismicity of the Andaman region, we operated 13 broadband seismic stations (Figure 1b). In the present work, we derive the crustal structure of Andaman Islands using joint inversion of receiver functions and surface wave dispersion measurements. This information was combined with global seismicity and CMT fault plane solutions to provide some insight into subduction model beneath Andaman Islands.

2. DATA AND METHODOLOGY

The data used in the present study was recorded by 13 broadband seismic stations operated in two different phases. During November 2003 to February 2004 (phase 1), we deployed 5 stations (orange triangles in Figure 1b), and during January to May 2005 (phase 2) we deployed 8 stations (red triangles). In phase 2, just after the 2004 Sumatra earthquake, we re-occupied 3 previous locations as in phase 1 (pink triangle). The seismological stations configurations included Guralp CMG-3T sensors with a flat velocity response between 0.008 – 50 Hz and REFTEK 130–01 data loggers. Data were continuously recorded at 50 samples per second and the corresponding Global Positioning System (GPS) time was logged.

Receiver function (RF), a well-known and established technique, was used to study the crustal structure of Andaman Islands. Receiver functions are radial and transverse waveforms created by deconvolving the vertical component from the radial and transverse components of the seismogram to isolate the receiver site effects from the other information contained in a teleseismic P- wave [Langston, 1979; Ammon, 1991; Liggoria and Ammon, 1999].

To compute receiver functions, teleseismic waveforms of the earthquakes with magnitudes above 5.5 and epicentral distances between 30° to 95° were selected. This epicentral range avoids multiple arrivals in the direct *P* wave field occurring at distances less than ~30° due to triplications caused by the rapid velocity increase in the upper mantle transition zone, and complications at distances greater than ~95° resulting from the core-mantle boundary. Figure 2 shows the location of earthquakes used in this study and recording station network. Due to geographical location of the study region, most of the earthquakes are from NE and SE directions.

We computed receiver function using iterative time domain deconvolution approach [Liggoria and Ammon, 1999]. Different Gaussian filter widths were tested, however, as our objective was to find the first order discontinuities, we preferred RFs with 1.6 Gaussian width, corresponding to low pass filter with a corner frequency at ~0.8 Hz. To further control the quality of waveform, we used only the RF with variance reduction cut-off above 80%. To equalize the effect of variable distances, RFs were moveout corrected to a reference slowness of 6.4 s/deg corresponding to an epicentral distance of 67° [Yuan et al., 1997] using IASP91 model. Out of total 1329 RFs calculated, only 269 good quality RFs were selected for further analysis. Figure 3 shows moveout corrected radial receiver functions calculated at individual seismic stations. IMD, RGT and HVL stations which operated during both the phases of experiment have maximum RFs, but due to technical problems HVL station could not record much earthquakes and produced lesser RFs.

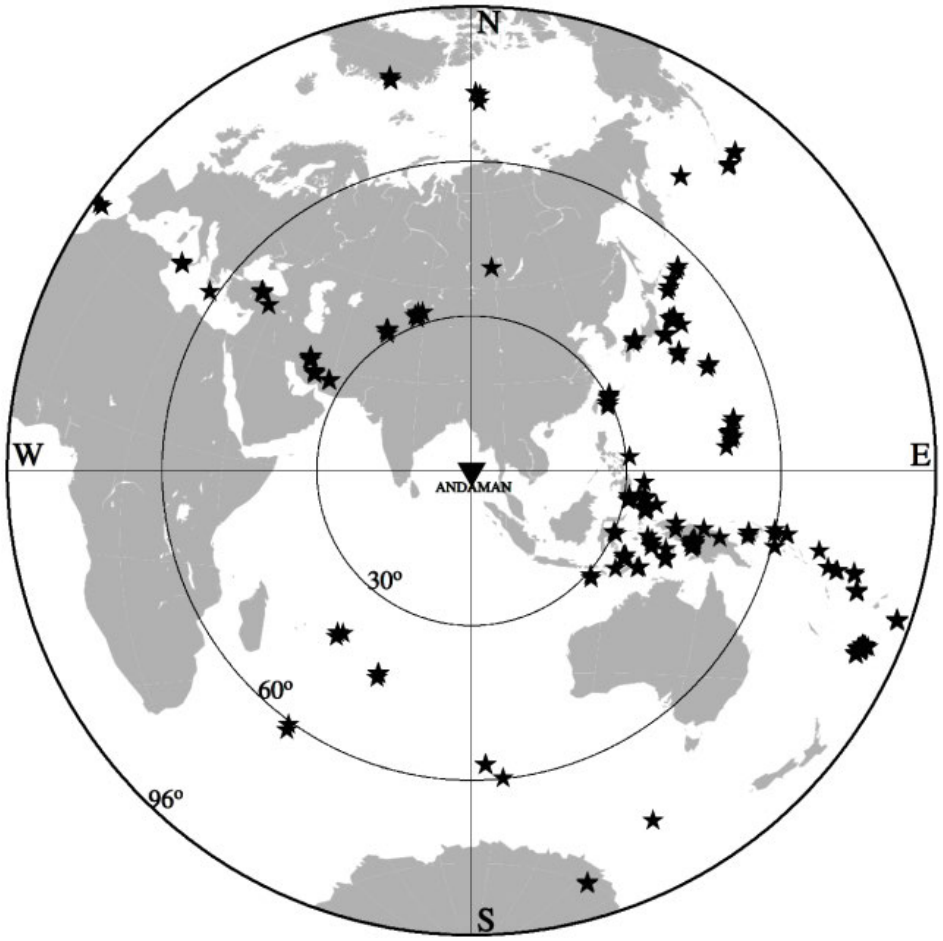

FIGURE 2. Epicentral locations of the teleseismic events (stars), Mb 5.8, used in this study. The triangle denotes Andaman seismic network.

Based on geographical setting, the whole study region is divided in three segments (North, Middle and South Andaman; Figure 1b); and the RF analysis is presented for these three segments.

2.1 NORTH ANDAMAN: [KGT]

RFs obtained at KGT (Kalighat) show a strong coherent phase (positive polarity) arriving at ~3.8 s. Other prominent observed phases (conversion and multiples) are at ~12-14 s and show strong back azimuthal dependence (Figure 3).

2.2 MIDDLE ANDAMAN: [TGP, RGT, BTG]

Both TGP (Tugapur) and RGT (Rangat) seismic stations in this part of Andaman show similarity in their waveform. Receiver functions at these stations show prominent phases (positive polarity) at ~2 s, ~5 s and ~13-14 s (Figure 3). Seismic station at BTG (Baratang), close to a mud volcano, exhibits complex RFs (Figure 3). This mud volcano erupted a huge volumes of slurry material after the main Sumatra-Andaman earthquake and the eruption has been associated with ascending fluids and gases at shallow subsurface level. At BTG, we found that the receiver functions from northern backazimuth (310° to 50°) events produces a visible shift in direct *P*. This shift in P could possibly be due to these low velocity layer at the subsurface below BTG. Other prominent visible phases are at ~4-5 s and ~10 s (Figure 3).

2.3 SOUTH ANDAMAN: [TIR, IMD, HTN, BTG, HVL, NIL]

The western station, TIR (Tirur) shows relatively simpler receiver functions with a strong coherent phase arriving at ~3.5 s, other phases (conversion and multiples) at ~5-6 s and ~15 s (not clear on all the RFs) (Figure 3). At central stations IMD (Portblair) and HTN (Hopetown) in this part of Andaman, we observed the Ps conversions at ~3 s, and this phase get shifted (~4.5 s) for NW direction (>270°) events (Figure 3). Other conversion at these stations include a strong phase at ~14 s. CHI (Chidiyatapu), the southernmost station, shows strong

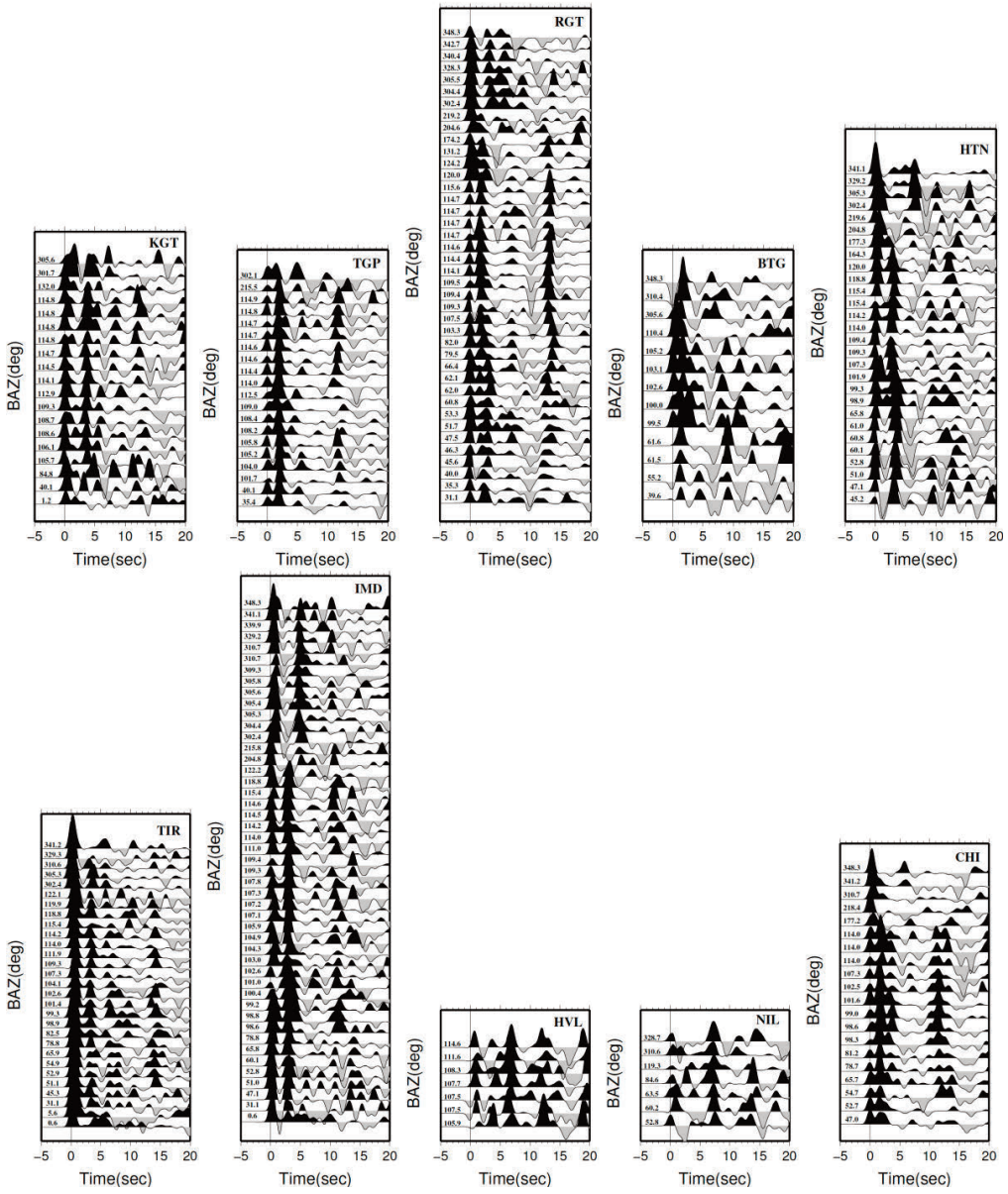

FIGURE 3. Equidistant plots of moveout corrected radial receiver functions calculated at individual stations and plotted with reference to backazimuth.

conversions at ~2 s and ~12 s (Figure 3). At the eastern stations HVL (Havelock) and NIL (Neil) in the south Andaman, we observed coherent phase at ~3-3.5 s with its multiple (PpPms) around ~12 s (Figure 3). One more strong conversion is observed at ~7 s with its multiple at ~20 s (Figure 3).

In general, the multiples are masked by various other phase(s), which makes it difficult to be distinguished at most of the stations. This is an inherent problem arising in complex subduction regions e.g., Cocos [Chang and Baag, 2007], Chilean [Dzierma et al., 2012], Korean [Kim et al., 2010], Sumatra [Macpherson et al., 2012]. Hence, we have restricted our analysis mainly based on clear conversions.

To study the nature of Moho conversions (Ps phase) and other intra-crustal phases, we have projected few RFs along the two profiles AA' and BB' (Figure 4a). These RFs were calculated for the earthquakes from SE direction (Figure 4b), recorded on majority of the stations and traversing similar ray path. These receiver functions were corrected for the distance moveout of the Moho converted Ps phase referenced to 67°. The average of the summed receiver function is presented (left and upper panel of Figure 4c and Figure 4d, respectively) and the individual receiver functions are plotted equi-spaced (right and bottom panel of Figure 4c and Figure 4d, respectively). Coherency of events at different stations can be very well tracked along both the profiles. A clear dif-

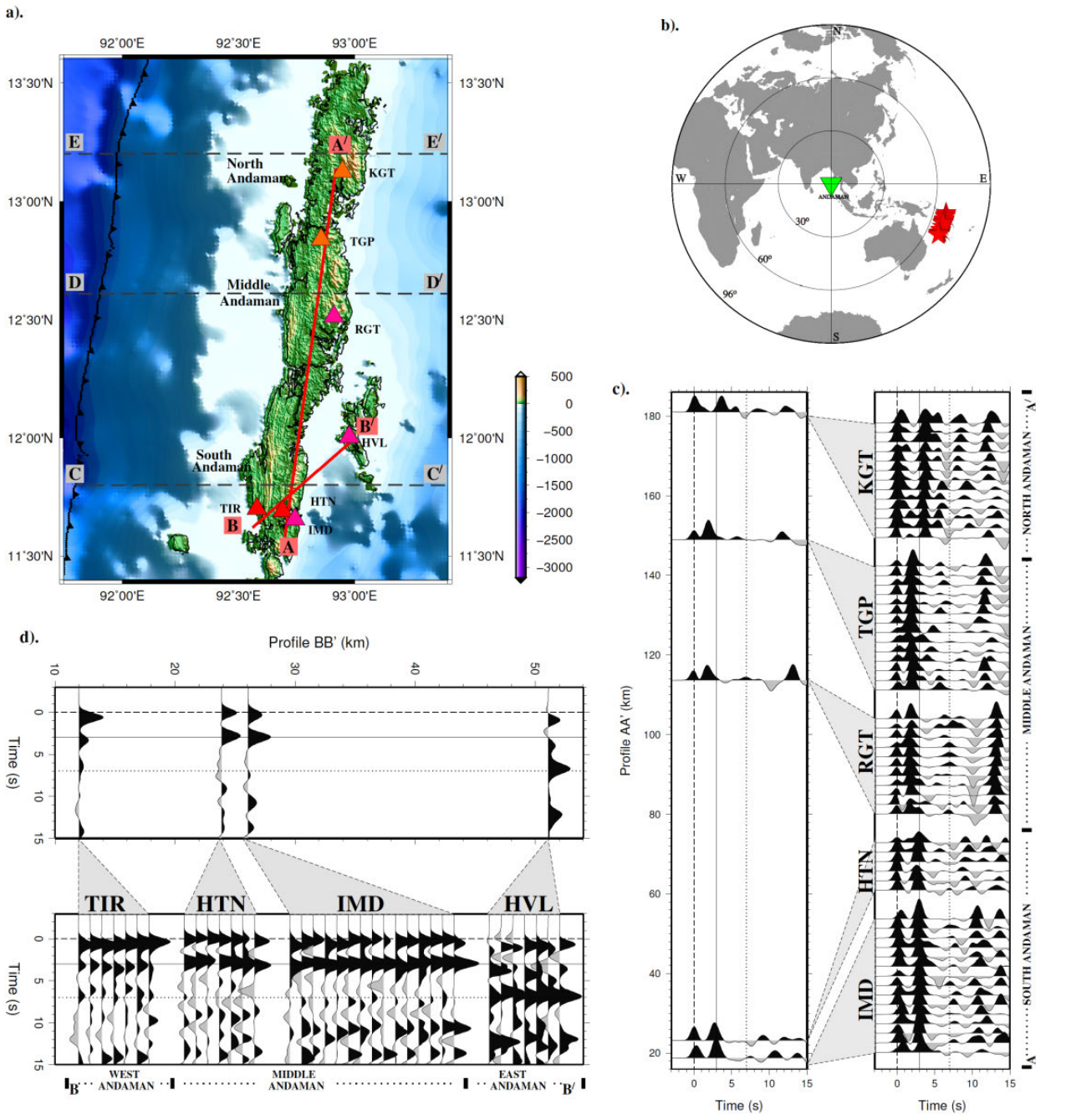

FIGURE 4. (a) Simplified map of study region showing profile locations used in Figs. 4c, 4d. (b) Andaman seismic network (inverted triangle) and earthquakes (red stars), from SE direction traversing similar path, used to calculate the moveout corrected receiver functions. (c) and (d) are plots of selected moveout corrected receiver functions projected along AA' and BB' (shown in Fig. 4a); where respective left panel shows the stacked receiver functions plotted as a function of relative distance along the particular profile with individual traces.

ference in Ps conversion along different segments of the Andaman arc is seen along a profile AA' (approx N-S direction) (Figure 4c). Variation in Ps arrival indicate differences in crustal topography along the three sectors of Andaman Islands. Similarly, there is significant variation in arrival of Ps conversion as we move across the width of Andaman in approximately E-W direction (profile BB'; Figure 4d). As we move away from trench to easternmost station (HVL), we observed a strong conversion arriving at around ~3 s. Due to limited data at this station we are unable to track its continuity. However, in consultation with neighbouring stations, we believe 3 s to be possible Ps from top crust and a strong conversion at 7 s could be from subducting Indian slab.

3. JOINT INVERSION

To obtain the seismic crustal structure beneath Andaman Islands, we have inverted the obtained radial receiver functions (RFs). The inversion of receiver functions is essentially a non-linear approach. Being a complex terrain, any additional weights to constrain inversion solution can provide reliability to results while converging towards the final solution. RFs are sensitive to the shear wave velocity contrast and has no control on the absolute shear velocity, whereas surface wave dispersion measurements constrain average shear velocity that reach deeper structure with increasing period. Since both RFs and surface wave dispersion are primarily sensitive to shear wave velocity, these can be inverted jointly to obtain a reliable estimate of shear velocity structure. Merging information from both receiver functions and surface wave dispersion into a single inversion algorithm limits the non-uniqueness inherent in receiver function and provides better constraints on shear wave velocity measurements.

Due to insufficient backazimuthal coverage of the earthquake, geographical location and duration of experiment, we could not analyze effect of dip, anisotropy, scattering etc. and restricted ourselves for the determination of simple 1-D velocity model beneath every station. Only selected receiver functions, sampling the similar ray path from a particular backazimuth (red stars in Figure 4b) were used for the joint inversion. Further, considering the complexity of terrain, we have inverted all individual receiver function at each station to obtain an average velocity structure. We used relatively small time window of 12 s for modeling to avoid any contamination due to multi pathing and other multiple phases.

Receiver functions and surface wave dispersion measurements were jointly inverted using iterative linearized damped least-square scheme [Julia et al., 2000; Herrmann and Ammon, 2004] which incorporates a priori smoothness constraints for velocities in adjacent layers. The 15 – 45 s period fundamental mode Rayleigh wave group velocities curves were extracted for each individual station in the Andaman region from surface wave tomography results of Acton et al. [2010]. Group velocity measurements represent an average picture of the region and cannot reflect the rapid change in structure of the region. Hence, a careful consideration was given for the sensitivities of each dataset towards underlying crustal structure and the size of the sampling region. Greater weight is given to fit the receiver function data during the joint inversion to obtain local structure beneath each seismic station. The joint inversion was performed for a range of weights and final models were selected based on the best fit to the receiver function, whilst maintaining an adequate fit to the dispersion data. In particular, model group velocities at short periods are allowed greater deviation from the observed group velocities to reflect the rapidly varying structures in the shallow part of crust.

In order to avoid biasing the inversion model, the starting model for the inversion at each of the sites was the same and consisted of the AK135 [Kennett et al., 1995] velocity model with the crust and sub-Moho mantle replaced with 4.48 km/s layers upto 60 km depth. The thickness of starting model was parameterized as homogeneous and isotropic layers of 1 km thickness until 34 km (2 km layer thereafter) to account for any velocity variation in the model for any possible variation in the subsurface velocity. A constant Vp/Vs value of 1.73 was assumed during each inversion as a starting point. Since receiver functions and surface wave dispersion measurements were inverted primarily for retrieving crustal structure, the model damping was chosen to be large for deeper mantle. Christensen and Mooney [1995] and Christensen [1996] has shown that shear wave velocity (Vs) in the lower crust cannot exceed 4.3 km/s, and Vs above this indicates the presence of lithology of mantle composition. Therefore, the depth where Vs >4.3 km/s was used as a marker to compute the Moho depth.

In order to test the robustness of our inversion results, the starting (input) model was perturbed by 5% of input velocity model and final output results were compared. As shown in Figure 5, perturbing the starting model has negligible effect on the final velocity models by the inversion process. In both the cases of velocity perturbation (increase or decrease), we could hardly find any significant variation in the output velocity models down to ~50 km depth; which shows the stability of the final inversion results.

The inversion results obtained from joint inversion of receiver function and surface wave dispersions at stations in different sectors of Andaman are presented in Figure 6. The velocity structure at seismic station (KGT, north Andaman) is well constrained with RFs and surface wave dispersion measurements (Figure 6, north Andaman). In Middle Andaman, TGP shows good matching between observed and modeled surface wave measurements, however RFs are not matched properly. In contrast, at RGT, RFs (observed and modeled) are well matched while, surface waves measurements have diversions at longer periods, however they are in $\pm 1\sigma$ error limits (Figure 6, middle Andaman). At seismic stations in south Andaman, RFs and surface wave disper-

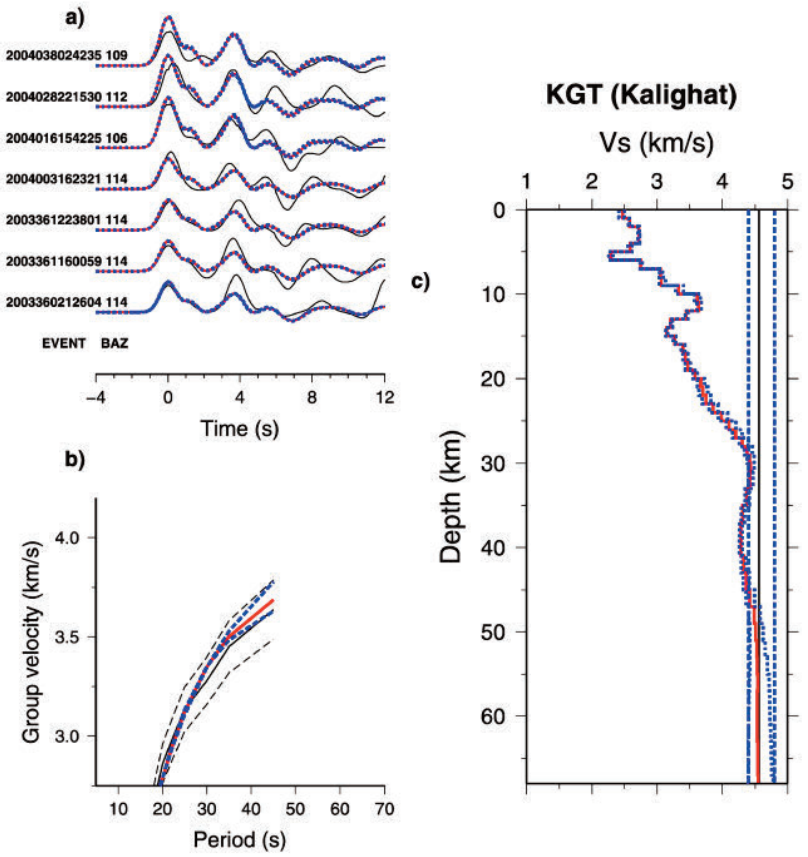

FIGURE 5. Effect on the inversion results when starting model is perturbed by 5%. (a) Observed RFs (Black), joint inversion results (Red) and effect on waveform due to perturbed starting model (dotted blue). (b) Observed group velocity (black) with error bounds (black dashed), joint inversion result (Red Solid) and group velocity dipersion due to perturbed input (Blue dotted). (c) Starting (black), final (red) and 5% perturbed (blue dotted) velocity model.

sion measurements (observed and modeled) are well matched and better constrained by the velocity model (Figure 6). At TIR (in east part of south Andaman) both RFs and surface waves dispersion curves are well modeled (Figure 6). At HVL (west part of south Andaman, we had lesser number of receiver functions. While surface wave measurements are well matched, RFs are not matched properly during modeling.

3.1 H-Vp/Vs STACKING METHOD

To quantify the crustal thickness and *Vp/Vs* ratio in the vicinity of each station, we modelled the amplitude and travel times of P-to-S conversions at the Moho (Ps) and its crustal multiples (PpPms and PpSms + PsPms) in the radial receiver function using the grid search algorithm [Zhu and Kanamori, 2000]. This algorithm has been successfully applied for obtaining Moho depths and Vp/Vs ratios for subduction zones e.g., Cocos [Chang and Baag, 2007], Korean [Kim et al., 2010] and Chilean [Dzierma et al., 2012]. This algorithm exploits the fact that arrival times and amplitude of specific Moho converted phases and multiples appearing on radial receiver functions are determined by known functions of Moho depth (*H*), Vp/Vs ratio. For a near true combination of *H* and *k* value, the quantity *S(H, Vp/Vs)* is defined as the weighted sum of the receiver function amplitudes at the calculated times of predicted arrivals of *Ps*, *PpPms* and *PpSms+PsPms* phases would be expected to be maximum.

$$S\,(H,\ Vp/Vs\ ) = w_1 r\,(t_1) + w_2 r\,(t_2) - w_3 r\,(t_3) \qquad (1)$$

where $r_j(t)$ is the amplitude of receiver function for the *j*th event, t_1, t_2, t_3 are predicted *Ps*, *PpPms* and *PpSms+PsPms* arrival times corresponding to Moho depth *H* and *Vp/Vs*. Since travel times used for crustal receiver function analysis are much sensitive to *Vs* than to *Vp*, we assume an average *Vp* (6.31 km/s, Pesicek et al. 2010*)* for the entire crust and perform the grid search for a large number of crustal models with varying thicknesses *H* (10 – 80 km) and varying *Vp*/*Vs* (1.6–2.0). Being a complex region, it was difficult to find well-defined global maximum and a strong trade-off existed between crustal thickness and Vp/Vs ratio (Figure 6d,

for each seismic station), therefore Moho depth obtained by joint inversion was used to obtain Vp/Vs ratio beneath each station. Figure 6d, shows the results of H - Vp/Vs for each station along with inversion results. From the present study, Vp/Vs ratio ranges from 1.79 to 1.83 for the entire study region. Due to limitation of the

NORTH ANDAMAN

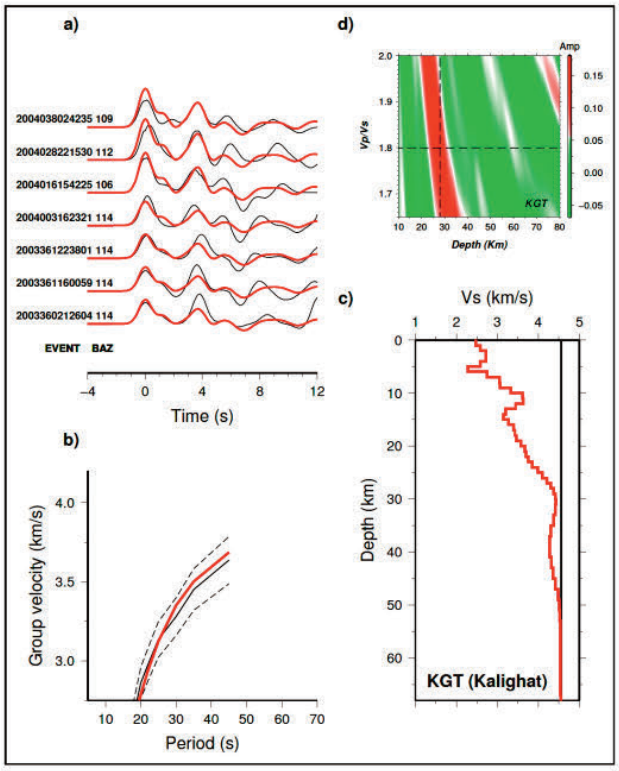

MIDDLE ANDAMAN

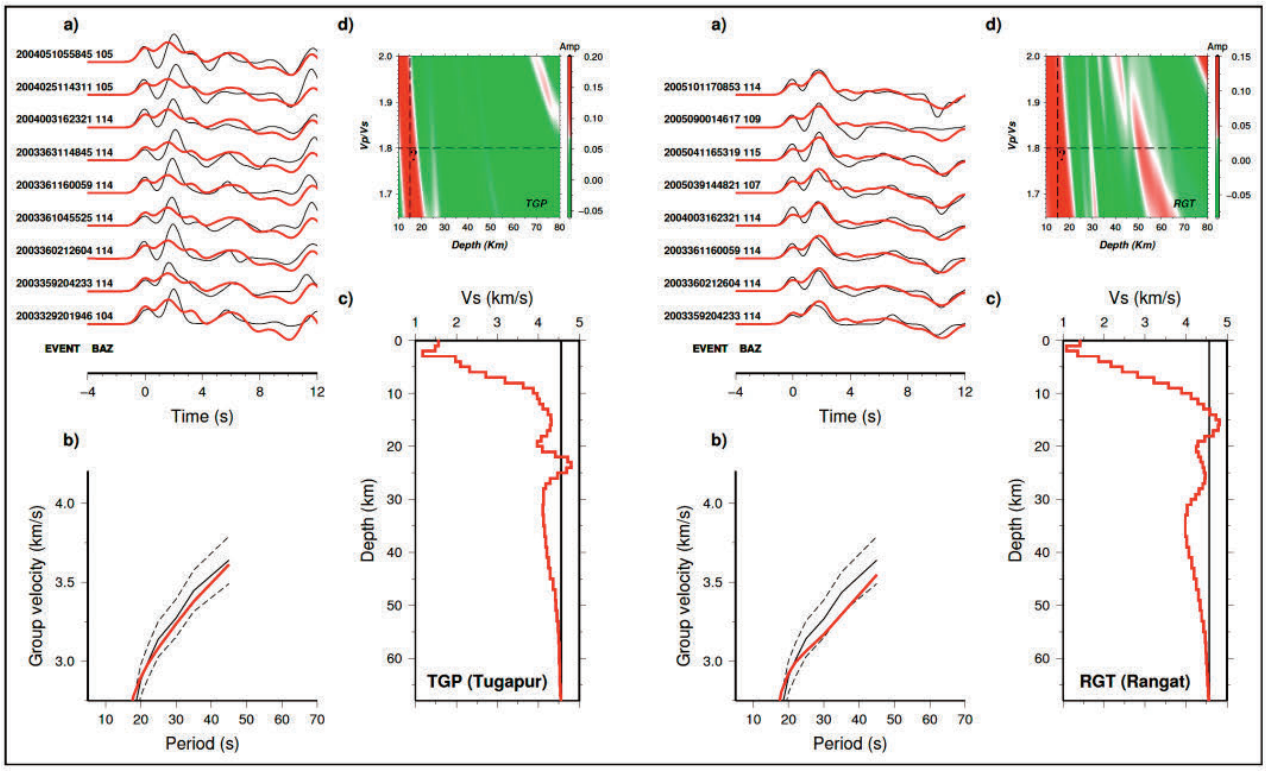

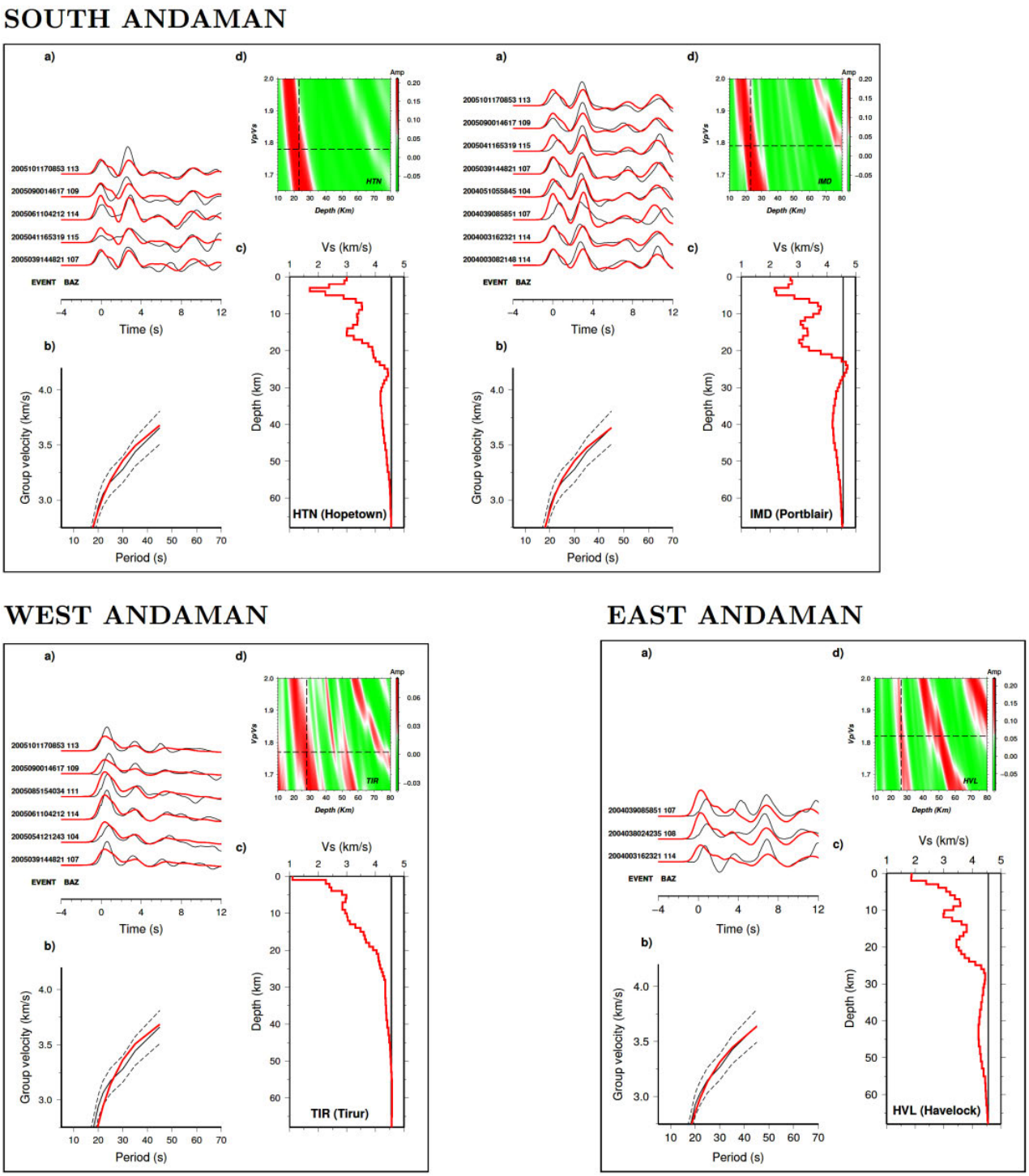

FIGURE 6. Inversion results using joint inversion of receiver function and surface wave for selected stations in North and Middle Andaman. (a) Observed (black) and synthetic (red from joint inversion) receiver functions. (b) Group velocity curves: observed (black), synthetic from joint inversion (red), and ±1σ error bounds (black dashed). (c) Initial (black) and final inverted (red) shear velocity models. (d) H–Vp/Vs stacking results.

datasets, it is very difficult to conclude the nature of curst, hydration or its level of saturation with fluids. However, possibilities of the presence of fluids generated by the metamorphism at deeper levels of curst in subduction zones [Peacock, 1990] cannot be ignored.

4. RESULTS AND DISCUSSION

To follow the geometry of the subducting slab, crustal thickness estimates obtained from joint inversion is interpreted together with hypocentral locations, fault

plane solutions and piercing points (using ray path of event-station pair). Hypocentral locations are obtained from high precision relocated earthquake from EHB catalogue (Engdahl et al. 1998, 2007), while fault plane solutions are from Harvard CMT (Centroid Moment Tensor) solutions (ISC 2010). Figure 7 shows the depth cross-sections along the profile EE' (North Andaman), DD' (Middle Andaman), CC' (South Andaman) (as shown in Figure 4a) obtained from seismicity, superimposed with our crustal depth estimates and focal mechanism solutions.

In the following section, we have discussed these results by diving Andaman Islands into three segments (North, Middle and South Andaman Islands).

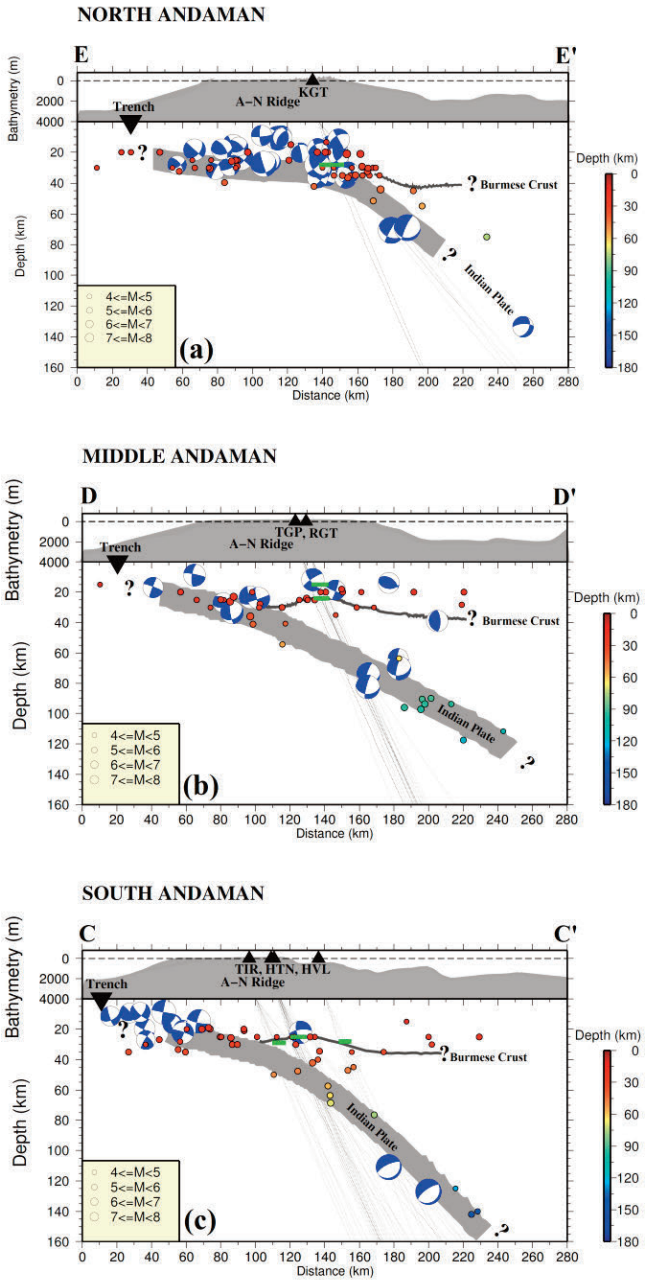

FIGURE 7. Vertical cross–sections across North, Middle and South Andaman, projected along three profiles (EE', DD' and CC' in Fig. 4a). The crustal estimates obtained from joint inversion are marked as green solid lines. Raypaths of events used for joint inversion are shown as thin lines (grey). The projected hypocenter locations (1960–2007) and focal mechanism solutions (M > 4.8) are taken from EHB Bulletin and Harvard CMT Solutions, respectively. For the convenience, the fault plane solution (the beach–ball) plots are as in a map view. The uncertainty or non availability of data is marked as "?". Inverted large black triangle and small vertical triangles on the Andaman bathymetry indicate the subduction trench and the seismic stations, respectively.

4.1 NORTH ANDAMAN

KGT (Kalighat), the northern seismic station in the Andaman Islands, shows a crustal thickness of ~28 km from joint inversion result. Top ~6-7 km is overlaid by thick low shear velocity (Vs ~2.5 km/s) Andaman flysch sediments (Figure 6d, North Andaman). Satellite gravity anomaly modeling and qualitative interpretation of RF results shows 30 km thick double oceanic crust, comprising 9 km Indian crust followed by 21 km Burmese crust (Rao et al., 2011). With gross crustal thickness (~28 km), our modeling results is in close agreement with Rao et al. [2011]. Depth cross-section plots along profile EE' (as shown in Figure 4a) was generated by combining the current modeling results with ray paths, seismicity and fault plane solutions (Figure 7a). As shown in figure 7a (North Andaman), the majority of the earthquakes occur in the depth range of ~10-30 km with main concentration around ~20-30 km. This shallow seismicity has mainly thrust dominated strike-slip motion. This could be due to the seismogenic coupling zone between subducting Indian slab and overriding Burmese crust, as shown by Grevemeyer and Tiwari [2006] and Shulgin et al. [2013] in the northern Sumatra. Focal mechanism solution reveals East (to North-East) gently dipping seismicity trend, which coincides with the direction of subducting Indian slab. The subducting slab has relatively low dip up to ~70 km from the trench and gets steeper further away from the trench. The shallow seismicity cluster is suggestive of intense tectonic deformation the subducting slab undergoes before descending into mantle. In absence of observed seismicity after ~70 km depth, except one earthquake at ~130 km depth, we can only guess the slab penetration in this part of Andaman.

4.2 MIDDLE ANDAMAN

In middle Andaman, both the seismic stations TGP (Tugapur) and RGT (Rangat) exhibit almost similar seismic structure (Figure 6d, Middle Andaman). At both the stations, two distinct interfaces (~15 and ~24 km depths) are observed. Based on RF analysis and modeling results, ~24 km is considered as the Moho depth (Figure 6d, Figure 7b). Below the Moho, shear velocity drops further (Vs ~ 4.0 km/s) and reaches back ~4.5 km/s at a depth of ~55 km (Figure 6d, Middle Andaman). Figure 7b shows the depth cross-section along profile DD' (as shown in Figure 4a), by combining modeling results with receiver function ray paths, known seismicity and fault plane solutions. The ~55 km interface could be signature from subduction Indian slab, being tracked down to a depth of ~120 km (Figure 7b). The low velocity between ~24 and 55 km could be interpreted as hydrated material sandwiched between the Burmese crust and subducting Indian slab. The earthquakes at a depth of about 100 km in the subducting Indian slab [Dasgupta et al., 2003] can be related to a phase transition in the slab causing fluid release and/or partial melting of the oceanic crust.

4.3 SOUTH ANDAMAN

Inversion result from TIR (Tirur), the western and closest station to the trench, shows the crustal thickness of ~28 km. HTN (Hopetown) and IMD (Portblair), in the central part of south Andaman segment, show crustal thickness of ~24 km. HVL (Havlok), the easternmost and farthest station from trench, shows a crustal thickness of ~26 km. Depth cross-section in this segment (Figure 7c, along profile CC' in Figure 4a) shows Indian slab is penetrating down to ~160 km. The slab convergence is more of an oceanic type as suggested by Subrahmanyam et al. (2008). Focal mechanism of earthquakes at depth >100 km is of normal type with low dipping eastward dominating strike, which can be related to plate bending deformation due to strong tensile (slab-pull) forces acting on subducting slab [Astiz et al., 1988; Conrad et al., 1999].

Crustal thickness obtained from joint inversion beneath the Andaman forearc region varies between ~24 and ~28 km. Joint inversion of receiver functions and surface wave dispersion measurements beneath Sumatra region also shows similar crustal thickness (Macpherson et al. 2012). Subsurface low shear velocity (Vs ~1.3 -2.5 km/s) layer, with an average thickness between ~4 and 7 km, is observed at almost all the seismic stations. This low velocity layer can be interpreted as thick soft Andaman flysch sediments. Magnetotelluric study in the region [Gokarn et al., 2006] also report similar sedimentary thickness. Average Vp/Vs ratio from ~1.79 to 1.83 represents accretionary hydrated oceanic crust with different level of saturation due to water released from downgoing slab as observed in other subduction zones [Peacock, 1990; Chang and Baag, 2007; Audet et al., 2009; Kim et al., 2010]. Earthquakes along the Andaman arc are mostly attributed to the ongoing subduction of Indian slab beneath the Burmese plate. The hypocenter distribution indicates a variable dip of the subducting Indian slab, similar to previous studies [Mukhopadhyay, 1988; Radhakrishna et al., 2008]. Seismicity, dip angle and focal mechanism solutions indicate a complex oblique convergence along the arc with transitional (continental - oceanic) type in the northern segment to oceanic type in the southern Andaman. Further south, in the 2005 Sumatra earthquake rupture area, the deep structural image using

seismic tomography modeling of wide-angle ocean bottom data also shows differences in the structure of the subduction system through crustal-scale changes (including crustal thickness change) and possible effects on the variations in the seismogenic behavior [Shulgin et al., 2013].

5. CONCLUSION

We investigate the crustal configuration of the Andaman Island using joint inversion of receiver functions and Rayleigh wave dispersion measurements. The crustal thickness varies between ~24 and 28 km in this region. In the entire region, a subsurface low velocity (Vs ~1.3 – 2.5 km/s) layer with varying thickness (~4 and 7 km) represents Andaman flysch sediments. Middle Andaman is more heterogeneous and has one prominent discontinuity at ~15 km. By combining derived crustal seismic structure with seismicity and CMT fault plane solutions; it is observed that the seismicity in the region is mostly related to the subduction Indian slab beneath the Burmese plate. The Indian slab is subducting at variable dip and down to variable depth. Along the Andaman arc, the convergence is complex; with transitional (continental-oceanic) type in the north Andaman to oceanic type in the south Andaman.

In the present study, we provide the information of the crustal seismic structure and subduction geometry in the Andaman region, however considering the complexity of the Andaman region, we find our dataset is limited and suggest a large scale multidisciplinary approach to examine and understand the 3-D structure, deep subduction and intrinsic processes beneath the Andaman and Nicobar Islands.

ACKNOWLEDGEMENTS. The presented results are the part of Ph.D. thesis of Santosh Mishra. Special thanks to Prof. Keith Priestley (Cambdridge, U.K.) for providing surface wave dispersion measurements and Prof. Bob Engdahl (Univ of Colorado, Boulder, U.S.A) for EHB dataset. The research was supported by Department of Science and Technology, New Delhi. We thank the Editor Prof. Saskia Goes and anonymous reviewers for their suggestions and comments for improving the quality of our manuscript.

REFERENCES

Acton, C. E., K. Priestley, V. K Gaur, S. S. Rai (2010). Group velocity tomography of the Indo-Eurasian Collision Zone, J. Geophys. Res., 115, 0148–0227.

Ammon, C. J. (1991). The isolation of receiver effects from teleseismic P, Bull. Seismol. Soc. Am., 81, 2504–2510.

Ammon, C. J., J. Chen, H. K. Thio, D. Robinson, N. Sidao, V. Hjorleifsdottir, H. Kanamori, T. Lay, S. Das, D. Helmberger, G. Ichinose, J. Polet, D Wald. (2005). Rupture Process of the 2004 Sumatra-Andaman Earthquake, Science, 308, 1133–1139.

Astiz, L., T. Lay and H. Kanamori, (1988) Large intermediate-depth earthquakes and the subduction process, Phys. Earth Planet. Inter., 53(1), 80-166.

Audet, P., M. G. Bostock, N. I. Christensen and S. M. Peacock (2009). Seismic evidence for overpressured subducted oceanic crust and megathrust fault sealing, Nature, 457, 76-78.

Bilham, R., R. Engdahl, N. Feldl and S. P. Satyabala, (2005). Partial and complete rupture of the Indo-Andaman plate boundary 1847-2004, Seismol. Res. Lett., 76(3), 299–311.

Chang, S. J. and C. E. Baag (2007). Moho Depth and Crustal Vp/Vs Variation in Southern Korea from Teleseismic Receiver Functions: Implication for Tectonic Affinity between the Korean Peninsula and China, Bull. Seism. Soc. Am., 97, 1621—1631.

Conrad, C.P., B. H. Hager (1999). Effects of plate bending and fault strength at subduction zones on plate, J. Geoph. Res., 104 B8, 17551—17571.

Christensen, N. I. (1996). Poisson's ratio and crustal seismology, J. Geophys. Res., 101, 3139-3156, doi:10.1029/95JB03446.

Christensen, N. I. and W. D. Mooney (1995). Seismic velocity structure and crustal composition of the lower crust: A global view, J. Geophys. Res., 100, 9761–9788, doi:10.1029/95JB00259.

Curray, J. R., (2005) Tectonics and history of the Andaman Sea region, J. Asian Earth Sci., 25, 055—078.

Curray, J. R., F. J. Emmel, D. G. Moore and R. W. Raitt (1982). Structure, tectonics and geological history of the northeastern Indian Ocean, pp. 399–450, 8, Plenum Press, New York

Dasgupta, S., M. Mukhopadhyay, A. Bhattacharya and T. K. Jana (2003). The geometry of the Burmese–Andaman subducting lithosphere, J. Seismol., 7, 155—174.

Dzierma, Y., M. Thorwart and W. Rabbel (2012). Moho topography and subducting oceanic slab of the Chilean continental margin in the maximum slip segment of the 1960 Mw 9.5. Valdivia (Chile) earthquake from P-receiver functions, Tectonophys., 530-531, 180–192.

Engdahl, E. R., R. van der Hilst and R. Buland, (1998). Global teleseismic earthquake relocation with improved travel times and procedures for depth determination, Bull. Seism. Soc. Am., 88, 722–743.

Engdahl, E. R., A. Villasenor, R. D. Heather and C. H. Thurber (2007). Teleseismic relocation and assessment of seismicity (1918– 2005) in the region of the 2004 Mw 9.0 Sumatra-Andaman and 2005 Mw 8.6 Nias Island great earthquakes, Bull. Seismol. Soc. Am., 97, S43–S61.

Franke, D., M. Schnabel, S. Ladage, D. R. Tappin, S. Neben, Y. S. Djajadihardja, C. Muller, H. Kopp and C. Gaedicke (2008). The great Sumatra-Andaman earthquakes - Imaging the boundary between the ruptures of the great 2004 and 2005 earthquakes, Earth Planet. Sci. Lett., 269, 118–130.

Gokarn, S. G., G. Gupta, S. Dutta and N. Hazarika (2006). Geoelectric structure in the Andaman Islands using magnetotelluric studies, Earth Planets Space, 58, 259–264.

Grevemeyer, I. and V. M Tiwari (2006). Overriding plate controls spatial distribution of megathrust earthquakes in the Sunda–Andaman subduction zone, Earth Planet. Sci. Lett., 251, 199–208.

Guzman-Speziale, M. and J. F. Ni (1996). Seismicity and active tectonics of the western Sunda Arc, in Tectonic Evolution of Asia, pp. 63–84, Cambridge Univ. Press, New York.

Herrmann, R. B. and C. J., Ammon, (2004). Computer Programs in Seismology, Surface wave, receiver functions and crustal structures, Saint Louis University, St. Louis, Missouri.

ISC, 2010, International Seismological Centre, On-line Bulletin, Int. Seis. Cent., Thatcham, United Kingdom, http://www.isc.ac.uk.

Ishi, M., P. M. Shearer, H. Houston and J. E. Vidale (2005). Extent, duration and speed of the 2004 Sumatra–Andaman earthquake imaged by the Hi-Net array, Nature, 435 (7044), 933–936.

Julia, J., C. J. Ammon, R. B. Herrmann and A. M. Correig (2000). Joint inversion of receiver function and surface wave dispersion observations, Geophys. J. Int., 143, 99–112.

Kamesh Raju, K.A., D. Ray, A. Mudholkar, G.P.S. Murty, V.K. Gahalaut, K. Samudrala, A.L. Paropkari, R. Ramachandran, L.S. Prakash (2012). Tectonic and volcanic implications of a cratered seamount off Nicobar Island, Andaman Sea, J. Asian Earth Sci., 56, 42-53.

Kennett, B., E. Engdahl and R. Buland (1995). Constraints on seismic velocities in the Earth from travel times, Geophys. J. Int, 122, 108–124.

Kennett, B. L. N. and P. R. Cummins (2005). The relationship of the seismic source and subduction zone structure for the 2004 December 26 Sumatra-Andaman earthquake, Earth Planet. Sci. Lett., 239, 1–8.

Khan, P. K. (2005). Variation in dip-angle of the Indian plate subducting beneath the Burma plate and its tectonic implications, Int. Geosci. J., 9, 227–234.

Kim, Y., R. W. Clayton and J. M. Jackson (2010). Geometry and seismic properties of the subducting Cocos plate in central Mexico, J. Geophys. Res., 115, B06310. doi: 10.1029/2009JB006942.

Langston, C. A. (1979) Structure under Mount Rainier, Washington, inferred from teleseismic body waves, J. Geophys. Res., 84(B9), 4749—4762.

Lay, T., H. Kanamori, C.J. Ammon, M. Nettles, S.N. Ward, A. Richard, S. L. Beck, S.L., Bilek, M.R. Brudzinski, R. Butler, H.R. DeShon, G. Ekstrom, K. Satake, S. Sipkin (2005). The Great Sumatra-Andaman Earthquake of 26 December 2004, Science, 1127-1133.

Liggoria, J. P. and C. J. Ammon, (1999). Iterative deconvolution and receiver function estimation, Bull. Seism. Soc. Am., 89, 1395–1400.

Macpherson, K. A., D. Hidayat, and S. H Goh (2012). Receiver function structure beneath four seismic stations in the Sumatra region, J. Asian Earth Sci., 46, 161—176.

Mishra S., S. Prajapati, S.S. Teotia, (2020) Mantle Transition Zones (MTZ) discontinuities beneath the Andaman Subduction Zone, J. Asian Earth Sci., 191, 104102, doi: 10.1016/j.jseaes.2019.104102.

Mishra, O. P., J. R. Kayal, G. K. Chakrabortty, O. P. Singh and D. Ghosh (2007). Aftershock investigation in Andaman–Nicobar Islands of India and its seismotectonic implications, Bull. Seismol. Soc. Am., 97(1A), S71–S85.

Mishra, O. P., D. Zhao, C. Ghosh, Z. Wang, O. P. Singh, B. Ghosh, K. K. Mukherjee, D. K. Saha, G. K. Chakrabortty and S. G. Gaonkar (2011). Role of crustal heterogeneity beneath Andaman-Nicobar Islands and its implications for coastal hazard, Natural Hazards, 57, 51–64.

Mukhopadhyay, M. (1984). Seismotectonics of subduction and backarc rifting under the Andaman Sea, Tectonophys., 108, 229–239.

Mukhopadhyay, M. (1988). Gravity anomalies and deep structure of Andaman arc, Marine Geophys. Res., 9, 197–210.

Nakajima, J., T. Matsuzawa, A. Hasegawa and D. Jhao (2001). Three-dimensional structure of and beneath northeastern Japan: Implications for arc

magmatism and fluids, J. Geophys. Res., 106, B10, 21,843-21,858.

Pal, T., P. P. Chakraborty, T. D. Gupta and C. D. Singh (2003). Geodynamic evolution of the outer arc-forearc belt in the Andaman Islands, The central part of the Burma-Java Subduction complex, Geol. Mag., 140, 289–307.

Peacock, S. M. (1990). Fluid processes in subduction zones, Science, 248, 329–337.

Pesicek, J. D., C. H. Thurber, S. Widiyantoro, H. Zhang, H. R. DeShon and E. R. Engdahl (2010). Sharpening the tomographic image of the subducting slab below Sumatra, the Andaman Islands and Burma, Geophys. J. Int., 182, 433–453.

Radhakrishna, M. and T. D. Sanu (2002). Shallow Seismicity, stress distribution and deformation pattern below Andaman-west Sunda arc and the Andaman Sea, northeast Indian Ocean, J. Seismol., 6, 25–41.

Radhakrishna, M., S. Lasitha and M. Mukhopadhyay (2008). Seismicity, gravity anomalies and lithospheric structure of the Andaman arc, NE Indian Ocean, Tectonophys., 460, 248–262.

Rao, N. P., C. N. Rao, P. Hazarika, V. M. Tiwari, M. R. Kumar, and A. Singh (2011). Structure and Tectonics of the Andaman Subduction Zone from Modeling of Seismological and Gravity Data, (Chapter.11) New Frontiers in Tectonic Research General Problems, Sedimentary Basins and Island Arcs, 249-268.

Replumaz, A., A. M. Negredo, S. Guillot and A. Villasenor (2010). Multiple episodes of continental subduction during India/Asia convergence: Insight from seismic tomography and tectonic reconstruction, Tectonophys., 483, 125–134.

Richards, S., G. Lister and B. Kennett. (2007). A slab in depth: Three-dimensional geometry and evolution of the Indo- Australian plate, Geochem. Geophys. Geosyst., 8 (12), 1–11.

Scotese, C. R., L. M. Gahaganand and R. L. Larson, (1988). Plate tectonic reconstruction of the Cretaceous and Cenozoic ocean basins, Tectonophys., 155, 27–48.

Shapiro, N. M., M. H. Ritzwoller and E. R. Engdahl, (2008). Structural context of the great Sumatra-Andaman Island earthquake, Geophs. Res. Lett., 35, L05301.

Shulgin, A., H. Kopp, D. Klaeschen, C. Papenberg, F. Tilmann, E.R. Flueh, D. Franke, U. Barckhausen, A. Krabbenhoeft, Y. Djajadihardja (2013). Subduction system variability across the segment boundary of the 2004/2005 Sumatra megathrust earthquakes, Earth and Planet. Sci. Lett., 365, 108-119.

Sorensen, M. B., K. Atakan and N. Pulido (2007). Simulated Strong Ground Motions for the Great M 9.3 Sumatra–Andaman Earthquake of 26 December 2004 January 2007, Bull. Seism. Soc. Am., 97, S139–S151.

Subrahmanyam, C., R. Gireesh, S. Chand, K. A. K. Raju, and D. G. Rao (2008). Geophysical characteristics of the Ninetyeast Ridge – Andaman island arc/trench convergent zone, Earth Planet Sci. Lett., 266, 29–45.

Yuan, X., J. N. Rainer, R. Kind, J. Mechie and E. Sandvol (1997). Lithospheric and upper mantle structure of southern Tibet from a seismological passive source experiment, J. Geophys. Res., 102, 27491–27500.

Zhu, L. and H. Kanamori (2000). Moho depth variation in southern California from teleseismic receiver functions, J. Geophys. Res., 105, 2969–2980.

*CORRESPONDING AUTHOR. Santosh MISHRA,
National Geophysical Research Institute (NGRI),
Hyderabad, India and PETRONAS Research Sdn. Bdg. (PRSB),
Exploration Technology, Group Research and Technology,
Product Delivery and Technology, Malaysia;
email: santosh.geoscience@gmail.com